Hydration of a Synthetic Clay with Tetrahedral Charges: A Multidisciplinary Experimental and Numerical Study

Emmanuel Rinnert,[†] Cedric Carteret,*[,‡] Bernard Humbert,[‡] Giovanna Fragneto-Cusani,[§] John D. F. Ramsay,[||] Alfred Delville,[⊥] Jean-Louis Robert,[▽] Isabelle Bihannic,[#] Manuel Pelletier,[#] and Laurent J. Michot[#]

Agence Nationale pour la gestion des Déchets RAdiocatifs, Parc de la Croix Blanche, 1/7 rue Jean Monnet, 92298 Chatenay Malabry CEDEX, France, Laboratoire de Chimie Physique et Microbiologie pour l'Environnement, UHP-CNRS UMR 7564, 405 route de Vandœuvre, 54600 Villers-les-Nancy, France, Institut Laue-Langevin, B.P. 156, 38042 Grenoble CEDEX France, Institut Européen des Membranes, CNRS-ENSCM-Université de Montpellier UMR 5635, 1919 route de Mende, 34293 Montpellier, France, Centre de Recherche sur la Matière Divisée, CNRS-Université d'Orléans UMR 6619, 1B rue de la Férollerie, 45071 Orléans CEDEX 2, France, Institut des Sciences de la terre d'Orléans, CNRS-Université d'Orléans UMR 6113, 1A rue de la Férollerie, 45071 Orléans CEDEX 2, France, and Laboratoire "Environnement et Minéralurgie", INPL-ENSG-CNRS UMR 7569, avenue du Charmois, BP40, 54501 Vandoeuvre CEDEX, France

Received: February 24, 2005; In Final Form: July 5, 2005

The interaction of water with a synthetic saponite clay sample, with a layer charge of 1 per unit cell (0.165 C m^{-2}), was investigated by following along water adsorption and desorption in the relative pressure range from 10^{-6} to 0.99 (i) the adsorbed amount by gravimetric and near-infrared techniques, (ii) the basal distance and arrangement of water molecules in the interlayer by X-ray and neutron diffraction under controlled water pressure, and (iii) the molecular structure and interaction of adsorbed water molecules by near-infrared (NIR) and Raman spectroscopy under controlled water pressure. The results thus obtained were confronted with Grand Canonical Monte Carlo (GC/MC) simulations. Using such an approach, various well-distinct hydration ranges can be distinguished. In the two first ranges, at low water relative pressure, adsorption occurs on external surfaces only, with no swelling associated. The next range corresponds to the adsorption of water molecules around the interlayer cation without removing it from its position on top of the ditrigonal cavity of the tetrahedral layer and is associated with limited swelling. In the following range, the cation is displaced toward the mid-interlayer region. The interlamellar spacing thus reached, around 12.3 Å, corresponds to what is classically referred to as a "one-layer hydrate," whereas no water layer is present in the interlayer region. The next hydration range corresponds to the filling of the interlayer at nearly constant spacing. This leads to the formation of a well-organized network of interlayer water molecules with significant interactions with the clay layer. The structure thus formed leads to a complete extinction of the d_{001} line in D_2O neutron diffraction patterns that are correctly simulated by directly using the molecular configurations derived by GC/MC. The next range ($0.50 < P/P_0 < 0.80$) corresponds to the final swelling of the structure to reach d spacing values of 15.2 Å (usually referred to the "two-layer hydrate"). It is associated with the development of a network of liquidlike water molecules more structured than in bulk water. The final hydration range at high relative pressure mainly corresponds to the filling of pores between clay particles.

I. Introduction

Despite numerous experimental and simulation studies, the structural and dynamical properties of water molecules in the interlayer spaces of smectite clay samples remain partially unknown. Most experimental work has focused on natural clays with octahedral charge deficit, i.e., montmorillonite and hectorite.[1] The different thermodynamical status has been characterized and quantified by water adsorption and immersion enthalpy measurements.[2−4] The evolution of swelling with water activity has generally been investigated using X-ray diffraction[2−7] or neutron diffraction.[8−10] The status of adsorbed water molecules has often been examined using vibrational spectroscopies under controlled water pressure[11−17] or NMR spectroscopy.[18−22] Finally, the dynamical properties can be derived from neutron scattering experiments,[10,23,24] dielectric measurements,[25−27] NMR relaxometry,[28,29] or echo attenuation under pulsed field gradient measurements.[30−31] These experiments tend to show that cation hydration is the main parameter controlling water uptake and swelling in montmorillonite and hectorite for water activities ≤ 0.98, i.e., under the so-called crystalline swelling regime.[6] This general picture is basically confirmed by numerous simulation studies[32−41] that can be used to study both the structural and dynamical properties of confined water molecules.

However, due to the important heterogeneity of natural clay samples, the interpretation of the results and comparisons

* Author to whom correspondence should be addressed. Tel.: 33 (0) 3 83 68 52 20. Fax: 33 (0) 3 83 27 54 44. E-mail: cedric.carteret@lcpme.cnrs-nancy.fr.
[†] Agence Nationale pour la gestion des Déchets RAdiocatifs.
[‡] Laboratoire de Chimie Physique et Microbiologie pour l'Environnement.
[§] Institut Laue-Langevin.
[||] Institut Européen des Membranes.
[⊥] Centre de Recherche sur la Matière Divisée.
[▽] Institut des Sciences de la terre d'Orléans.
[#] Laboratoire "Environnement et Minéralurgie".

10.1021/jp050957u CCC: $30.25
Published on Web 11/18/2005

between them can sometimes be difficult. For instance, the existence of interstratified states of various hydrated layers in Wyoming montmorillonite[2−4] could either be truly due to thermodynamics or result from the existence in the sample of various layers having different compositions and charges. In addition, the complexity of the layer structure of natural clay samples can be a drawback for molecular simulations as it makes the choice of a representative layer structure rather difficult. For these reasons, the use of synthetic clay samples appears as a fruitful alternative for a proper understanding of the physical chemistry of clay minerals.[42] In that context, we recently used a series of synthetic saponites of general formula $(Si_{8-x}Al_x)$-$Mg_6O_{20}(OH)_4Na_x$ with $0.70 \leq x \leq 2.0$.[43−49] In such swelling clay minerals, the charge is located in the tetrahedral layer, i.e., close to the interlayer domain. Thus, the oxygen atoms located close to the tetrahedral substitution sites that bear a negative charge could represent binding sites for water molecules. Furthermore, the use of such a series of synthetic samples allows for the study of the influence of layer charge on the behavior of clay minerals. In the present paper, we will focus on one synthetic saponite sample exchanged with sodium cations with a layer charge of 1.0 per unit cell (i.e., 0.165 C m^{-2}) that we will study through the combination of a wide range of experimental approaches and Monte Carlo simulation procedures. We will show that information obtained from the different techniques must be confronted to obtain a clear picture of the hydration behavior of swelling clay minerals.

II. Experimental Details

Synthesis. The synthetic saponite sample was prepared by Jean-Louis Robert at ISTO (Orléans, France) by a hydrothermal treatment of hydrolyzed gels prepared by coprecipitation of Na, Mg, Al, and Si hydroxides at pH = 14, according to a slightly modified version of the gelling method of Hamilton and Henderson.[50]

The source of Na was sodium carbonate; the sources of Al and Mg were titrated solutions of their nitrates. The source of Si was $(C_2H_5O)_4Si$ (TEOS). The initial composition corresponding to the stoichiometry of the target saponite was hydrolyzed by the slow addition of ammonia until a gel was obtained. This resulting gel was slowly dried up to ∼200 °C. It was then calcined at 600 °C by further temperature increase. The calcined material was crushed for homogenization. It was then introduced in Morey-type externally heated pressure vessels in which the samples are insulated from the vessel wall by a silver coating. The hydrothermal reactor was then heated at 400 °C under a 1000 bar water pressure. Samples were recovered after four weeks. ^{29}Si and ^{27}Al NMR confirmed the single-phase character.[51,52] The resulting structural formula is: $Na_x(Si_{8-x}Al_x)$-$(Mg_6)O_{20}(OH)_4$, with $0.7 \leq x \leq 2.0$ The sample used in this study is characterized by a layer charge of 1 per unit cell. The mean particle size deduced from low-pressure high-resolution argon adsorption measurements is around 250 nm.[47]

Methods. *Water Vapor Gravimetric Adsorption* experiments were carried out in LEM using a lab-built quasi-equilibrium setup designed around a Setaram MTB 10-8 symmetrical microbalance.[52] Water vapor was supplied to the sample (thermostated at 30 °C) from a source kept at 45 °C at a slow flow rate to ensure quasi-equilibrium conditions at all times. The simultaneous recording of mass uptake and equilibrium pressure (gauge 0−100 Torr) directly yielded the water vapor adsorption isotherm. The experimental conditions were a sample mass of around 100 mg and an outgassing at 110 °C during 18 h under a residual pressure of 0.01 Pa.

X-ray Diffraction under Controlled Water Vapor Pressure. The evolution of X-ray diffraction patterns with water relative pressure was followed in LEM using a specially designed experimental device. An oriented sample of saponite mixed with kaolinite used as an internal nonswelling reference (5% kaolinite in the mixture) was placed inside a chamber, allowing for the control of relative humidity and temperature. The chamber, kept at 30 °C, was connected to a water vapor source. The water relative pressure in the chamber was controlled by changing the temperature of the source. An Edwards capacitive pressure gauge (0−1000 mbars) was placed on the chamber for direct pressure measurements. Using this double measurement, an accuracy of ±0.01 could be obtained on relative pressure measurements. X-ray diffraction patterns were recorded simultaneously over 30° (θ) on an Inel CPS 120 curved detector using transmission geometry with Co Kα radiation. This geometry did not allow us to obtain an accuracy on d_{001} values better than ±0.1 Å. The sample was outgassed before the experiment at 30 °C under a residual pressure of 0.1 Pa during 24 h. For each hydration state, equilibrium was checked by recording the evolution of X-ray diffraction patterns with time. The time for equilibrium was variable between 2 and 4 h, depending on the hydration pressure.

Neutron Diffraction under Controlled Water Vapor Pressure. Neutron diffraction diagrams were obtained on beamline D16 at the Institut Laue-Langevin in Grenoble, France. To vary the contrast between clay-layer and interlayer water, diffractograms were collected for both H_2O and D_2O. The saponite powder was first treated under vacuum at 110 °C, and the outgassed samples were suspended in pure D_2O in a glovebox under a dry nitrogen atmosphere. The samples were then centrifuged in sealed tubes, and the centrifugate was redispersed in pure D_2O. The final suspension was placed in sealed tubes stored in a dry nitrogen atmosphere. The clay suspension was then used to deposit thin oriented films on aluminum slides. Six aluminum slides were stacked for each experiment to obtain an acceptable signal/noise ratio. The slides were placed on a goniometric head inside a humidity chamber, allowing for the control of water vapor relative pressure.[53] Neutron diffraction diagrams were then obtained in the reflection mode along the desorption isotherm. At the end of the experiment, the sample was opened to the atmosphere, and the humidity chamber was filled with H_2O. The experiments were then carried out again with H_2O along the desorption isotherm. The wavelength used was 4.54 Å, and the angular range, covered in a $\theta/2\theta$ geometry, varied between 4 and 65° (θ). The use of a bidimensional detector covering a window of 7° (2θ) allowed us to examine the samples in a q range from 0.019 to 2.50 $Å^{-1}$. For the D_2O diagrams, three patterns with steps of 1° (θ) and counting times of 100 s per point were accumulated. For H_2O diagrams, only two recordings were accumulated in the same conditions.

Near Infrared Diffuse Reflectance Spectra under Controlled Water Pressure were obtained in LCPME on a Perkin-Elmer 2000 FTIR spectrometer with a deuterated triglycine sulfate (DTGS) detector, a tungsten−halogen source, and a quartz beam-splitter. Working in the near-infrared region has several significant advantages for studying the status of adsorbed water molecules: (i) It allows us to work with pure mineral powders without any need for dilution in a nonabsorbing matrix. We recently showed that KBr could interfere with Na-saponite.[46] (ii) It provides a quantitative analysis that could never be obtained in the mid-IR region. Indeed, in that latter wavenumber range, the extinction coefficients of OH modes are strongly linked to the strength of H-bonds.[54] In contrast, in the NIR

region, the extinction coefficients are almost constant, which allows linking water adsorbed amounts with the integrated area of IR bands.[55−57] (iii) In the case of clay minerals in the mid-IR region, it is rather difficult to determine unambiguously the position of OH stretching bands of adsorbed water due to significant overlap and broadening of the OH stretching bands both with each other and with structural ν-OH bands (e.g., refs 14 and 50). In the NIR region, the separation between structural OH groups and water OH groups is enhanced, allowing for easier and more precise band assignments. The spectrum resolution was 8 cm^{-1}. Diffuse reflectance spectra were recorded from 8000 to 4000 cm^{-1} and obtained by the coaddition of six individual scans. Ground potassium bromide powder dried under vacuum (10^{-3} Pa) at 30 °C was used as a reference (R_0 signal). The reflectance spectra are displayed in $-\log(R/R_0)$, where R corresponds to the diffuse reflection collected on the sample. Water relative pressure control was carried out by fixing the sample temperature and by controlling the temperature of a water source connected to the experimental cell using a lab-built Peltier device. This device allowed us to cover the range of $5 \times 10^{-7}-0.99$ relative water pressure at 30 °C.[58] Additional pressure control was provided by an absolute capacitive gauge (Edwards 0−100 Torr, with an accuracy of 10^{-2} Torr) that measures the pressure in the adsorption cell. Before the experiment, the sample was outgassed at 100 °C under a residual pressure of less than 10^{-3} Pa, using a two-stage pump formed with a scroll pump for primary vacuum and a turbomolecular pump for secondary vacuum. The whole pumping system was oil-free to avoid any pollution by organics. For each hydration state, equilibrium was checked by recording the evolution of spectra with time. The time for equilibrium was variable between 1 and 6 h, depending on the water pressure. Reproducibility of the experiments was checked by carrying out three water adsorption−desorption isotherms.[58]

Raman Scattering Spectra under Controlled Water Pressure were collected in LCPME on a Jobin-Yvon T64000 spectrometer equipped with an optical microscope, a threefold monochromator, and a nitrogen-cooled CCD camera. The excitation was induced by a laser beam of an argon Spectra Physic Laser Stabilité 2017 at a wavelength of 514.5 nm. The beam was focused using a long-frontal ×50 objective (numerical aperture = 0.5) on an area of about 3 μm^2. The laser power on the sample was approximately 20 mW. The backscattered Raman spectra were collected in a confocal mode to avoid optical artifacts, particularly the collection of parasite signals coming from the glass window placed on top of the sample. The spectral resolution was 3 cm^{-1}, with a wavenumber precision better than 1 cm^{-1}. Wavenumber calibration was obtained by recording the green-emission ray light of a Hg lamp. The saponite sample used in this study, being white, laser-induced heating of the sample, was very limited as checked by Raman Stokes−anti-Stokes measurements. Water pressure control was achieved using the exact same cell as that used for infrared experiments.

Grand Canonical Monte Carlo Simulations were performed[59,60] at CRMD to determine the amount of confined water molecules as a function of the water partial pressure and the interlamellar separation determined by X-ray diffraction. The simulation cell was composed from three clay lamellae, each containing 24 unit cells. The atomic coordinates of the ideal $Si_8Mg_6O_{20}(OH)_4$ unit cell were identified with that of phlogopite.[61] The tetrahedral substitution sites were selected randomly in each clay layer using an exclusion rule; i.e., two aluminum atoms cannot be present in the same ditrigonal cavity and fully compensated by the intralamellar sodium counterions. The clay/water and clay/cation atomic potentials and electric charges (Table 1) were derived from previous quantum calculations.[31] The clay/water potential results from the sum of electrostatic, repulsive, and dispersive contributions:

TABLE 1: Parameters Used for the Grand Canonical Monte Carlo Simulations

	Si	Mg	O_1	O_2	H	Al
q_i (e)	−2.67	−1.413	1.36	0.95	−0.295	−1.67
b_{iO} (Å^{-1})	4.83	4.83	3.32	3.32	2.45	4.83
b_{iH} (Å^{-1})	8.77	8.77	2.45	2.45	5.26	8.77
b_{iNa} (Å^{-1})	3.33	3.33	3.33	3.33	3.33	3.33
D_{iO} (MJ/mole)	417	417	75	75	7.2	417
D_{iH} (MJ/mole)	10	10	7.2	7.2	200	10
D_{iNa} (MJ/mole)	74	74	74	74	74	74
A_{iO} (MJ/(mole Å^{-2}))	1.2	1.2	−1.1	−1.1	2.4	1.2
A_{iH} (MJ/(mole Å^{-2}))	−0.6	−0.6	0.55	0.55	−1.2	−0.6
C_{iO} (MJ/(mole Å^{-6}))	0.68	0.0	2.5	2.1	0.40	0.68
C_{iH} (MJ/(mole Å^{-6}))	0.14	0.0	0.48	0.40	0.08	0.14
C_{iNa} (MJ/(mole Å^{-6}))	0.13	0.0	0.46	0.39	0.06	0.13

$$E_{\mathrm{el+rep}} = \sum_{i=1}^{N_{\mathrm{wat}}} \sum_{j=1}^{N_{\mathrm{at}}} \left[\frac{q_i q_j}{4\pi\epsilon_0 \epsilon_r r_{ij}} + D_{ij} \exp(-b_{ij} r_{ij}) + \frac{A_{ij}}{r_{ij}^2} \right] \quad (1)$$

where N_{wat} stands for the oxygen and hydrogen atoms of the water molecule and N_{at} stands for those of the clay particle. As shown in the Table 1, the A_{ij} parameters were selected to fully compensate each other ($A_{iH} = -0.5A_{iO}$ and $\sum_{j=1}^{N_{\mathrm{at}}} A_{jO} = \sum_{j=1}^{N_{\mathrm{at}}} A_{jH} = 0$), restricting the long-range behavior of that contribution to an effective r^{-4} term, ensuring its convergence. The atomic charge and the geometry of the water molecules were those of the TIP4P water model ($q_O = 1.04$ e).[62] The dispersion contributions matched the soft-core repulsion of our quantum potential and were evaluated from the atomic polarizabilities estimated on the basis of the net atomic charges:[30]

$$E_{\mathrm{disp}} = -\sum_{i=1}^{N_{\mathrm{wat}}} \sum_{j=1}^{N_{\mathrm{at}}} \frac{C_{ij}}{r_{ij}^6} \left[1 - \left(\sum_{k=0}^{6} \frac{(b_{ij} r_{ij})^k}{k!} \right) \exp(-b_{ij} r_{ij}) \right] \quad (2)$$

The clay/sodium potential was derived in the same manner by focusing on the leading contribution from the oxygen atoms of the clay network (Table 1). This model of the clay/water interaction is fully compatible with the TIP4P model of bulk water[63] in addition to the sodium/water potential.[64] Ewald summation[65] was used in addition to the 3D minimum image convention to ensure the convergence of the electrostatic contribution by using 2196 replicas for the summation in the reciprocal space and a damping parameter in the direct space set to 0.19 Å^{-1}, leading to an accuracy of better than 0.002.[66]

The (00l) components of the diffraction pattern of the confined sodium ions (noted N_{cat}) and the different atoms of the water molecules (noted N_{wat}) were directly evaluated from their equilibrium configuration during the GC/MC simulations. For that purpose, 9000 wavenumbers were uniformly generated in the reciprocal space between 0 and 2.7 Å^{-1} for the calculation of the diffracted amplitude:

$$I(q_z) = S^*(q_z) S(q_z) \quad (3a)$$

with

$$S(q_z) = \sum_{i=1}^{N_{\mathrm{wat}}+N_{\mathrm{cat}}+N_{\mathrm{at}}} f_j(q_z) \exp[i q_z (\vec{r}_j)_z] \quad (3b)$$

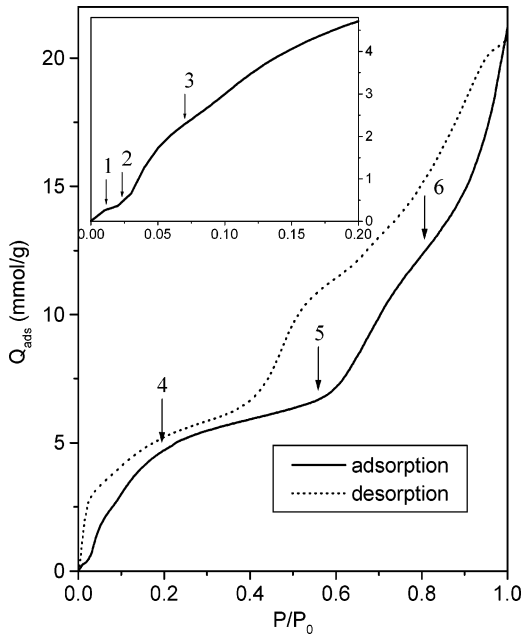

Figure 1. Water adsorption−desorption isotherm obtained at 303 K on the saponite sample.

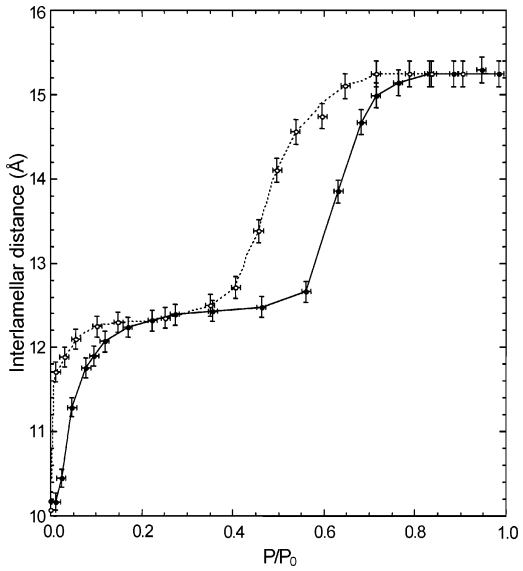

Figure 2. Evolution with water relative pressure of the interlamellar distance measured by X-ray diffraction for the saponite sample.

The net atomic charge and q-dependence of the X-ray structure factors were reproduced from tabulated data.[66] The diffracted amplitudes were corrected for the polarization factor of the X-ray scattering $(1 + \cos^2 \theta)/2$ and the Lorentz factor $1/(\sin^2 \theta \cos \theta)$ corresponding to the Bragg−Brentano experimental setup for both the X-ray and neutron scattering experiments.[68,69]

III. Results

The water adsorption−desorption isotherm of the saponite sample obtained at 303 K is presented in Figure 1. Compared with the water adsorption isotherm obtained for Wyoming Na-montmorillonite,[1,2] the curves exhibit much sharper features with well-defined steps and pseudoplateaus. At a very low relative pressure, the adsorption isotherm increases sharply, up to a relative pressure of around 0.01 (first arrow in the insert). This first increase is followed by a small plateau, extending up to a relative pressure of around 0.025 (second arrow in the insert). The adsorbed quantity then rises sharply to reach 5 mmol/g for a relative pressure of ∼0.20. An inflection point located around $P/P_0 = 0.07$ and $Q_{ads} = 2.6$ mmol/g can also be noticed in this range (third arrow in the insert). For $0.25 \leq P/P_0 \leq 0.60$, the isotherm displays a pseudoplateau, where the amount of water adsorbed increases slightly. For higher relative pressures, a second step is observed in which the adsorbed amount reaches ∼13 mmol/g. Finally, at a high relative pressure, the isotherm displays an important increase in adsorbed volume. The desorption branch exhibits a significant hysteresis with a similar evolution as in adsorption except for the very low-pressure range. The hysteresis at medium relative pressure, ∼0.50, can tentatively be attributed to the presence of mesopores in the clay film.[49] In contrast, the low-pressure hysteresis is linked to structural features.[49]

The evolution of basal spacing with water relative vapor pressure, estimated from the position of the d_{001} X-ray line, is presented in Figure 2. The pattern observed follows the water adsorption isotherms, with strong increases in d spacing corresponding to the steps observed on the water adsorption isotherms and nearly constant d spacings in ranges where the water adsorbed amount varies only marginally. Compared with sodium montmorillonite,[1,2] the various steps are much more marked. Such a feature has already been observed for other clays with tetrahedral charge localization.[70−76] Under vacuum, the basal distance is close to 10.1 Å. In the very first adsorption stages, for $P/P_0 \leq 0.03$, no swelling higher than 0.1 Å is observed. The first step observed on the water adsorption isotherm corresponds to the first swelling stage at the end of which basal spacings values of around 12.5 Å are obtained. Such values can be assigned to a "one-layer hydrate". However, it must be pointed out that no definite distance can be associated with this stage as the distance changes continuously between 12.2 and 12.6 Å for $0.20 \leq P/P_0 \leq 0.55$. In the second swelling stage, the basal spacing grows to a value of 15.2 Å and remains constant thereafter. The previous hysteresis observed on the gravimetry water adsorption isotherms is reproduced in the evolution of basal distances both at medium and at low relative pressures.

Neutron diffraction diagrams obtained along the desorption isotherm are presented in Figure 3 for H_2O (Figure 3A) and D_2O (Figure 3B). The basal distances are coherent with those derived from X-ray experiments. Strong differences between the diagrams, corresponding to H_2O desorption and D_2O desorption, can be observed. Indeed, in the case of H_2O, the d_{001} reflection is by far the most intense, and there are very little changes in the relative intensities corresponding to the various harmonics. In contrast, in the case of D_2O, the relative intensities of the different lines vary strongly with water relative pressure. A particularly striking illustration of this feature can be observed in the transition between the "two-layer hydrate" and the "one-layer hydrate", where the d_{001} reflection located around 12.5 Å is completely extinguished whereas the 002 reflection at 6.26 Å keeps a strong intensity. The d_{001} reflection reappears for lower relative pressure.

Figure 4 presents the evolution of the near-infrared spectra with increasing water pressure. Two main regions corresponding to water signals can be observed on the spectra. The first domain between 4500 and 5500 cm^{-1} corresponds to the combination of water stretching modes $(\nu_{OH})_w$ and water bending mode (δ_{HOH}). The second one around 7000−7300 cm^{-1} corresponds to combinations and overtones of various $(\nu_{OH})_w$ as well as overtones of ν_{OH} of structural hydroxyl groups. In the NIR region, the signals corresponding to structural hydroxyls and

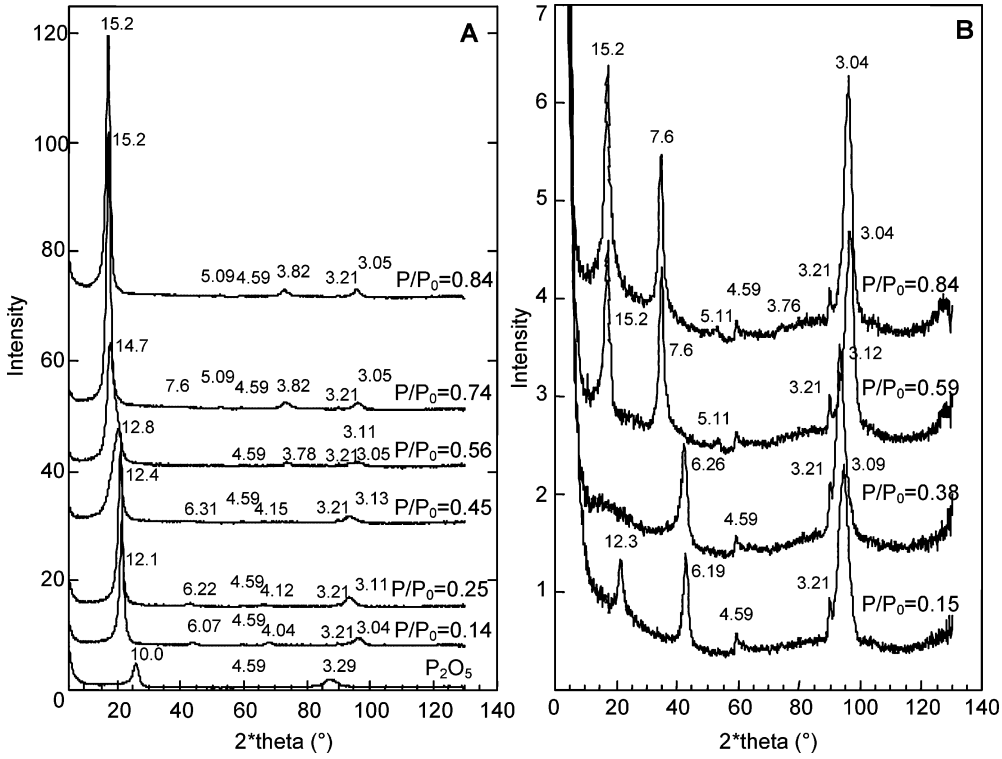

Figure 3. Neutron diffraction patterns obtained in desorption for saponite. (A) H_2O and (B) D_2O.

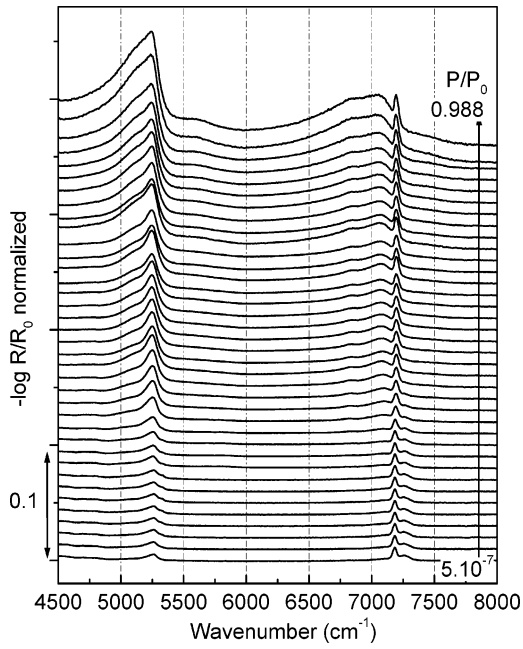

Figure 4. Near-infrared spectra under different water relative pressures, from 5×10^{-7} to 0.988.

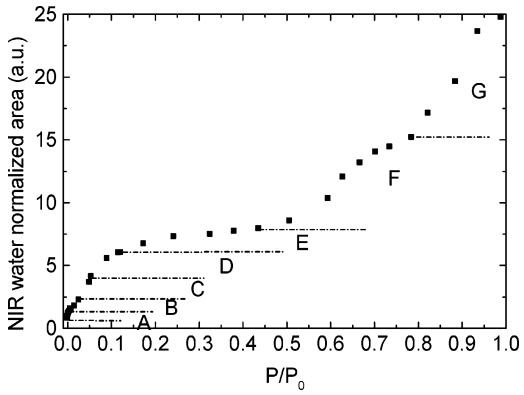

Figure 5. Water adsorption isotherm obtained by near-infrared diffuse reflectance spectroscopy, at 30 °C. Integration of combination bands of water from 4500 or 4750 to 5500 cm^{-1}.

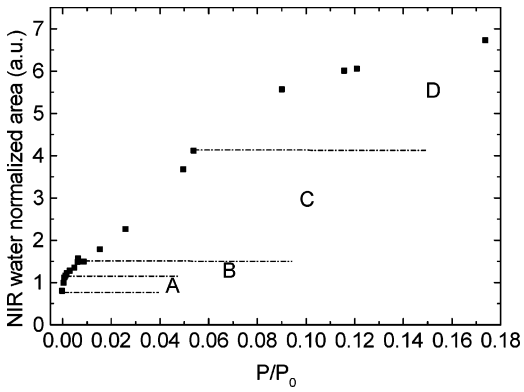

Figure 6. Low relative-pressure enlargement of the water adsorption isotherm presented in Figure 5.

to water are much more discriminated than in the mid-IR region.[48,55−57,77−79] In addition, as already mentioned, quantitative information can be obtained in the near-infrared region. Indeed, after normalizing the spectra on the combination $\nu+\delta$ modes of structural hydroxyls groups at 4350 cm^{-1}, the integration of the signals between 4500 and 5500 cm^{-1} is proportional to the amount of adsorbed water.[55−57] Figure 5 presents the evolution of the normalized integrated area as a function of water relative pressure, and Figure 6 shows an enlargement in the low relative pressure range. The shape of the adsorption isotherm thus derived is very close to that obtained from gravimetric measurements (Figure 1), and it allows us to distinguish different regions where water uptake changes significantly, as discussed in the following sections.

The water adsorption−desorption isotherm obtained by GC/MC simulations, taking into account the evolution of inter-

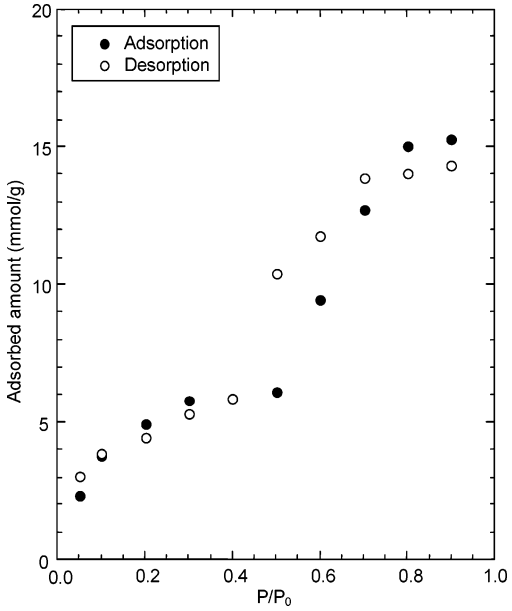

Figure 7. Water adsorption−desorption isotherm obtained by GC/MC simulations.

lamellar distances obtained from XRD measurements (see above), is displayed in Figure 7. The adsorption−desorption isotherm thus derived is very close to those obtained by either gravimetric measurements (Figure 1) or NIR experiments (Figure 5), which validates the choice of parameters displayed in Table 1. A slight discrepancy is observed at high relative pressures, which will be discussed in the discussion section.

IV. Discussion

The various experimental results obtained allow the definition of various well-defined relative pressure ranges in the swelling behavior of the synthetic Na-saponite. The molecular phenomena associated with each range can be studied in more detail on the basis of data derived from experimental and simulation results.

Initial State of the Sample. The infrared spectrum corresponding to the sample after outgassing at 100 °C under a vacuum of 0.1 Pa (Figure 8A, spectrum a) reveals that under those conditions (basal distance around 10 Å), the saponite sample still contains significant amounts of water. This was also previously shown by controlled transformation rate thermal analysis.[49] The amount of water still present in the sample accounts roughly for half of a water molecule per sodium cation.[49] In the spectral region corresponding to water, the infrared spectrum displays two components at 5260 and 5170 cm^{-1}. The difference between those two wavenumbers suggests that the water molecules still present under vacuum possess two identical OH bonds.[78−80] The water molecule symmetry is then C_{2v} with two hydrogen atoms similarly perturbed. The observed wavenumbers are lower by approximately 70 cm^{-1} compared to those for water in the vapor state,[81] and the intensity of the component at 5170 cm^{-1} is relatively high, which may reveal the influence of the dielectrical properties in the confined interlayer space. These remaining water molecules can then be seen as isolated molecules strongly linked to the interlayer Na^+ cations. In the region corresponding to structural hydroxyl groups (Figure 9A, spectrum a), two bands can clearly be observed at 7185 and 7260 cm^{-1}. Though noisy, the Raman spectrum (Figure 10B, spectrum a) in the fundamental OH stretching range 3600−3750 cm^{-1} also exhibits two components at 3675 and 3712 cm^{-1}. The mode at 3675 and the corresponding overtone located at 7185 cm^{-1} correspond to unperturbed OH groups whereas the second modes at 3712 and 7260 cm^{-1} correspond to OH groups perturbed by the presence of a Na^+ cation, located close to the ditrigonal cavity.[46,48] The peak height ratio between the two types of components yields the layer charge of the sample. However, the signals corresponding to perturbed OH groups are rather wide in both Raman and infrared, and the area ratios between the two bands approximately yield twice the layer charge. Therefore, it can be suggested that in the dry state, each sodium cation perturbs two structural hydroxyl groups, the width of the signal revealing a different perturbation of the two OH groups.

First Hydration Range. At the very beginning of the adsorption isotherm (Figures 1 and 6), the adsorbed quantity increases sharply up to 0.13 mmol/g for a relative pressure of 1.5×10^{-3}. In this relative pressure domain, no swelling is observed by XRD (Figure 2). The infrared spectrum corresponding to such a pressure is presented in Figure 8A, spectrum b. The associated spectral evolution can be more clearly observed on the difference spectrum (Figure 8B, difference α). In this first hydration range, two signals grow at 5320 and 5150 cm^{-1}. Such a difference in wavenumber of 170 cm^{-1} characterizes a water molecule in which one OH bond absorbing at a high wavenumber is free of H-bonding, whereas the second one, absorbing at a lower wavenumber, is hydrogen bonded.[78−80] The appearance of those water signals is associated to a small shift of the nonperturbed structural hydroxyls, noticeable in Figure 9B, difference α, by an S-shaped profile centered at 7185 cm^{-1}. The water molecules adsorbed in this step can then be tentatively located on the edge faces of the clay particles, where they would bind to edge Mg−OH groups. Such an interpretation is partially validated by the evolution in the high wavenumber region where the structural hydroxyls appear to be marginally affected. In addition, considering the lateral surface area of the saponite sample,[47] the adsorbed quantity in this stage would correspond to approximately 10 water molecules per nm^2 on the edge faces, which is coherent with a cross sectional area of 10.6 $Å^2$ for water molecules adsorbed in this range.[82] However, considering the amount of Mg−OH sites on the edge faces, such a value appears a bit too high, which may be due to the presence on the edge faces of small micropores, due to the imperfect stacking of clay layers.

Second Hydration Range. In the range of relative pressure between 1.5×10^{-3} and 0.02, the adsorbed quantity increases only slightly (Figures 1 and 6) to reach a value of around 0.3 mmol/g. In this pressure domain, the interlamellar distance remains constant as nearly no swelling is observed by XRD experiments (Figure 2). The infrared spectrum obtained in the range 4500−6000 cm^{-1} (Figure 8A, spectrum c) displays two additional signals at 5245 and 5100 cm^{-1} that can be clearly observed on the difference spectrum (Figure 8B, difference β). In parallel, in the range corresponding to structural hydroxyls and water overtones, the main changes observed are linked to the appearance of a signal around 7080 cm^{-1} (Figure 9B, difference β). Small modifications of the signals of the structural hydroxyls are also revealed by a W-shaped profile centered at 7205 cm^{-1}. The observed wavenumbers in the domain corresponding to H_2O combinations are typical of water molecules interacting with a cation.[11,12,14] Still, as no swelling occurs in this range, it can be proposed that the observed bands correspond to water molecules interacting with the external surface cations. The spectral evolution around 7200 cm^{-1} can then be assigned to a decrease of the perturbation of external OH groups by external Na^+ cations. Taking into account the structural charge

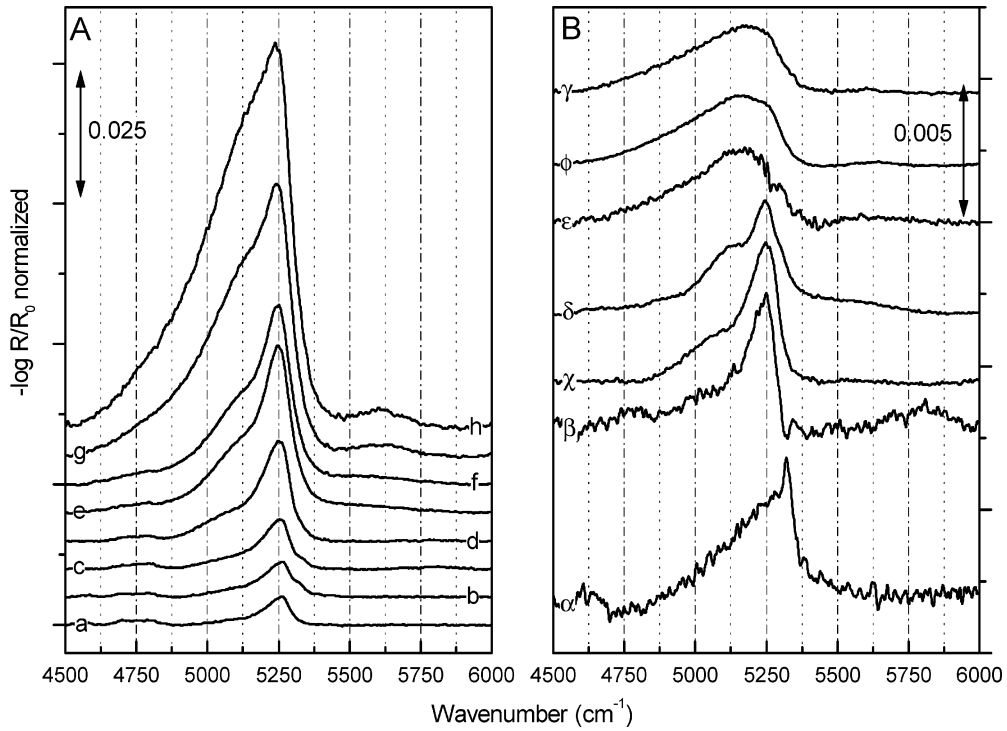

Figure 8. (A) Near-infrared diffuse reflectance spectra under different water relative pressures in the range of combination bands of water: a: 5×10^{-7}; b: 1.5×10^{-5}; c: 0.015; d: 0.050; e: 0.174; f: 0.436; g: 0.785; h: 0.936. (B) Difference spectra: α is the difference between b and a spectra from (A).

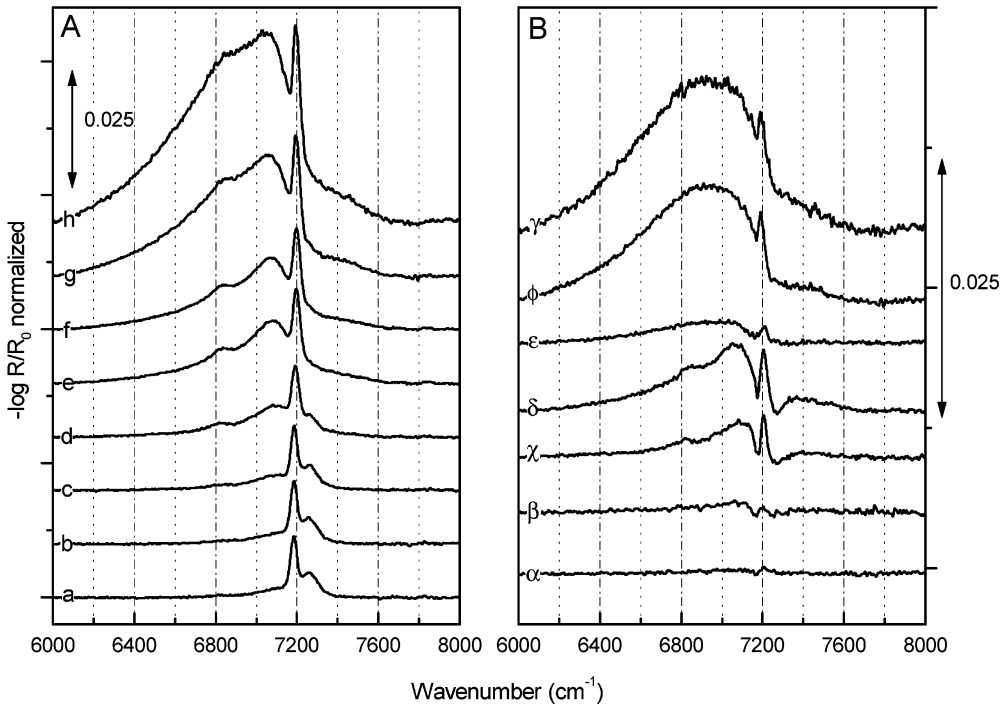

Figure 9. (A) Near-infrared diffuse reflectance spectra under different water relative pressures in the range of overtones bands of water and structural hydroxyls: a: 5×10^{-7}; b: 1.5×10^{-5}; c: 0.015; d: 0.050; e: 0.174; f: 0.436; g: 0.785; h: 0.936. (B) Difference of spectra: α is the difference between b and a spectra from (A).

and the external basal surface area deduced from low-pressure argon adsorption,[47] the total amount of water molecules adsorbed in this stage would correspond to about 6 water molecules per external cation, i.e., a complete hydration sphere on the external surfaces. The initial adsorption of water molecules on external Na^+ cations before any swelling is a feature that has been previously observed in the case of montmorillonite (e.g., refs 2, 3, 15, and 83). In most cases, it was deduced on the basis of observed adsorbed water amounts that were higher than those calculated from interlayer water only. In the present study, the detailed NIR analysis coupled with other experimental techniques allows the observation of the specific signature of these water molecules. Furthermore, it appears that tetrahedral charge location significantly reduces the relative water pressure range on which water molecules adsorb on the external surfaces only (up to $P/P_0 \approx 0.20$ for Wyoming Na-montmorillonite.[2] This difference can be tentatively linked to differences in the initial state of the sample under vacuum, saponite exhibiting a basal

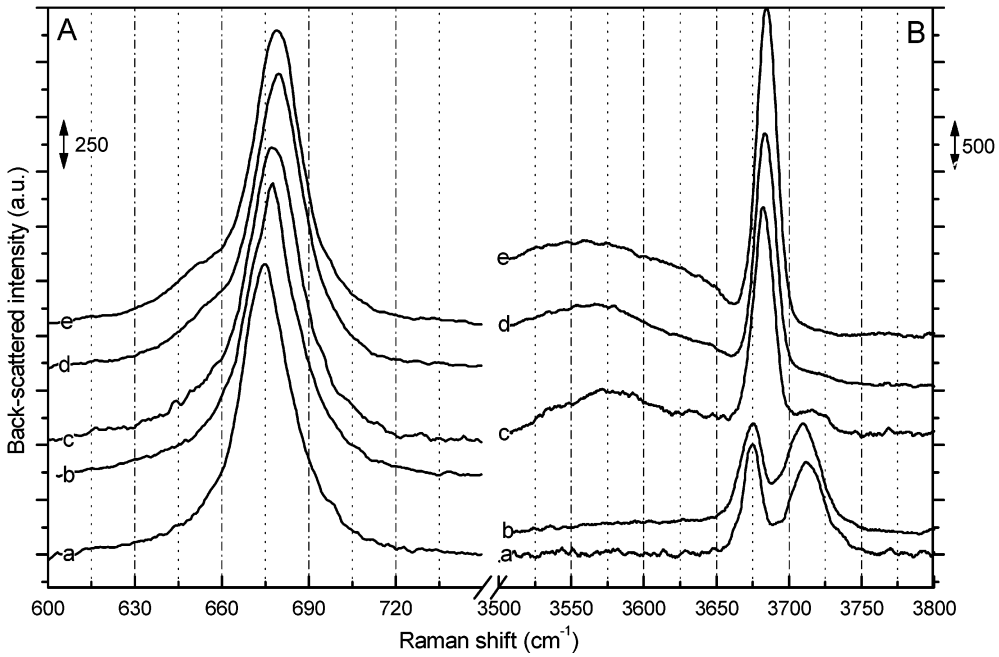

Figure 10. Raman backscattered spectra under different water relative pressures in the range corresponding to fundamental symmetric stretching of Si−O−Si and Si−O−Al (600−750 cm^{-1}) (A) and corresponding to fundamental stretching of structural hydroxyls and water (3500−3800 cm^{-1}) (B). a: 4×10^{-7}; b: 0.043; c: 0.091; d: 0.135; e: 0.266.

spacing around 10.2 Å, i.e., ≈0.6 Å higher than in the case of montmorillonite (≈9.6 Å).

Third Hydration Range. In the third hydration range for P/P_0 between 0.02 and 0.06, the adsorbed quantity increases strongly to reach a value of around 2.5 mmol/g (Figure 1). The adsorbed amount in this range then corresponds to 2.2 mmol/g. During that stage, a first swelling is observed with an interlamellar distance of 11.3 Å for $P/P_0 = 0.05$ (Figure 2). This stage is accompanied by a strong increase of the infrared signals at 5245 and 5100 cm^{-1} (Figure 8B, difference χ), i.e., at the same spectral position as in the previous hydration range. In parallel, in the domain corresponding to structural hydroxyls and water overtones (Figure 9A, spectrum d and Figure 9B, difference χ), two signals grow at 7080 and 6820 cm^{-1} (Figure 9B, difference χ), the peak at 7185 cm^{-1} shifts slightly toward 7190 cm^{-1} (Figure 9A, spectrum d), and the intensity of the band at 7265 cm^{-1} decreases slightly. For a slightly lower relative pressure (0.04), the Raman spectra in the range 600−800 cm^{-1} and 3500−4000 cm^{-1} (Figure 10) reveal modification neither on the symmetrical Si−O−Si stretching around 674 cm^{-1} [84,85] nor in the range of structural hydroxyls around 3710 cm^{-1}. The IR signals observed in this hydration range display the same signature as those observed in the previous one, and can then be assigned to water molecules linked to the Na^+ cation. In view of the swelling observed and of the important increase in adsorbed amount, it can be deduced that this stage corresponds to the beginning of the hydration of the internal cations. Considering the structural formula of the synthetic saponite sample, this stage involves the adsorption of 1.7 water molecules per sodium cation. As the Raman spectra do not exhibit any significant change around 3700 and 670 cm^{-1}, and considering the limited swelling of the sample, it can be proposed that, in this stage, water molecules adsorb around the cation without modifying its position relative to the clay layer. In that context, the observed interlamellar distance of 11.3 Å, could correspond to a true distance rather than to the interstratification between a zero-layer hydrate and a "one-layer hydrate". It must be pointed out that the GC/MC simulation carried out for a relative pressure of 0.05 (Figure 7) yields the correct adsorbed amount, which could be used as an indirect evidence for the existence of a defined hydration state in this region. Whatever its exact origin, this "intermediate" swelling stage must be considered as real as we are working with a synthetic sample in which layer heterogeneity is certainly limited.

Fourth Hydration Range. For relative pressures between 0.06 and 0.18, the adsorbed quantity increases strongly again to reach an amount of 4.5 mmol/g, which then corresponds to the additional adsorption of 2 mmol/g, i.e., ∼1.5 water molecule per cation. Concomitantly, the basal spacing reaches a value of 12.3 Å that is classically assigned to a "one-layer hydrate" state.[73] This confirms that the transition to the full "one-layer hydrate" is associated with the solvatation of the interlayer cation by 3 water molecules, as already deduced in the case of hectorite by IR spectroscopy.[11] In this water relative pressure range (Figure 8B, difference δ), four near-IR components grow in the range 4500−6000 cm^{-1} at 5130, 5245, 5310, and 5550 cm^{-1}. In parallel, in the wavenumber range 6000−8000 cm^{-1}, two water signals grow at 6835 and 7080 cm^{-1} (Figure 9B, difference δ), whereas the signal corresponding to structural OH groups perturbed by interlayer cations vanishes; the signal corresponding to unperturbed OH groups initially located at 7185 cm^{-1} shifts toward 7195 cm^{-1} (Figure 9A, spectrum e). The changes observed in the range corresponding to structural hydroxyl stretching modes can be interpreted as corresponding to the "expulsion" of the sodium cations from their location on top of the structural hydroxyls in the middle of the ditrigonal cavities. In the range of water combination modes, the band at 5245 cm^{-1} and its companion at 5100 cm^{-1} (whose existence can be inferred from the width of the IR signal between 5050 and 5200 cm^{-1}) can be assigned, as in the previous stages, to water molecules interacting with the sodium cation. The signals at 5310 and 5130 cm^{-1} then correspond to a new kind of water molecule in which one OH group is hydrogen bonded and the other one is rather free of hydrogen bonding.[78,80] It can then be assigned to water molecules located between two other water molecules, as already proposed for water molecules adsorbed on previously adsorbed water molecules at silica surfaces.[78,79]

Such an assignment is coherent with the appearance of libration modes around 5550 cm^{-1}. As this hydration stage involves the adsorption of approximately two water molecules per sodium cation, it could be proposed that the first of those two molecules is characterized by the signals at 5245 and 5100 cm^{-1}, whereas the second one can be linked to the bands at 5310 and 5130 cm^{-1}. A confirmation of this interpretation is obtained from Raman spectra. Indeed, for relative pressures between 0.045 and 0.095 (spectra b and c in Figure 10B), the region corresponding to structural hydroxyls is strongly modified, whereas the changes are only marginal between 0.095 and 0.22 (spectra c and d in Figure 10B). In parallel, the wavenumber corresponding to the Si−O−Si stretching mode around 674 cm^{-1} shifts strongly between 0.045 and 0.095 (spectra b and c in Figure 10A), which can be assigned again to the sodium cation leaving the ditrigonal cavity. The changes are less marked for higher relative pressure. Such an expulsion of the sodium cation from the ditrigonal cavity was already inferred from IR spectroscopy measurements[86] in the case of montmorillonite. However, in the present study, working with a synthetic trioctahedral mineral allows us to unambiguously evidence this mechanism and to assign it precisely to the adsorption of a third water molecule around the sodium cation.

The GC/MC simulations obtained for relative pressures of 0.10 and 0.20 (Figure 11) are coherent with the previous interpretation. Indeed, for $P/P_0 = 0.10$, nearly all sodium ions are surrounded by three water molecules with very few water molecules linked to each other, whereas for $P/P_0 = 0.20$, water molecules linking 2 hydrated sodium ions start to be observed. In parallel, some hydrogen-bond network starts becoming visible, which agrees with the libration signal observed around 5550 cm^{-1}. A comparison between experimental ($P/P_0^{desorption} = 0.15$) and calculated ($P/P_0^{adsorption} = 0.20$) neutron diffraction patterns for both H_2O and D_2O are shown in Figure 12. The neutron diffraction patterns were recorded in desorption, but it was previously shown[49] that, if one considers adsorbed amount, adsorption and desorption patterns are equivalent in the ranges of P/P_0 between 0 and 0.5 and between 0.75 and 1. Furthermore, NIR spectra obtained for the same adsorbed amount in adsorption or desorption have been shown to be strictly equivalent.[57] Therefore, diffractograms recorded in desorption for a relative pressure of 0.15 should be equivalent to diffractograms recorded in adsorption for $P/P_0 = 0.20$ (Figure 1). In the case of H_2O (Figure 12A), the agreement between experimental and calculated patterns is very good (except for the width of the peak that derives from the choice of the number of diffraction layers made in the simulation), whereas some discrepancy in relative intensities is observed for D_2O. This slight discrepancy could well be due to the existence of small amounts of interstratified states, which was recently evidenced in the same saponite samples by high-resolution X-ray diffraction studies.[87]

Fifth Hydration Range. For relative pressures between 0.18 and 0.45−0.50, the water adsorbed amount increases less steeply (Figure 1) to reach a value of around 6.2 mmol/g, corresponding to the adsorption of 1.3 additional water molecules per sodium cation. In parallel, the interlamellar distance increases only slightly to reach a value of 12.5 Å (Figure 2). In this water relative pressure range, the difference IR spectrum in the domain 4500−6000 cm^{-1} (Figure 8B, difference ϵ) displays a very broad asymmetrical massive centered around 5160 cm^{-1} and a discontinuity at 5250 cm^{-1} that is interpreted as resulting from the disappearance of the component at 5245 cm^{-1} observed in the previous hydration stage. In addition, difference ϵ exhibits a significant absorption below 5000 cm^{-1} that was never observed in the previous hydration ranges. In parallel, libration signals increase at 5580 cm^{-1}. This set of spectral results indicates the development in the interlayer of a disordered percolating hydrogen bond network. The asymmetry toward low wavenumbers characterizes rather strong H-bonds, which is coherent with the adsorption of additional water molecules in a confined space. In the range corresponding to water and hydroxyl stretching overtones, broad bands are observed around 6900 cm^{-1}, whereas a narrow signal appears at 7210 cm^{-1} (Figure 9B, difference ϵ). The existence of this latter signal suggests an increased repulsive perturbation of the structural hydroxyl compared with that of the previous hydration step, which can be assigned to the presence of water molecules located close to the ditrigonal cavity.

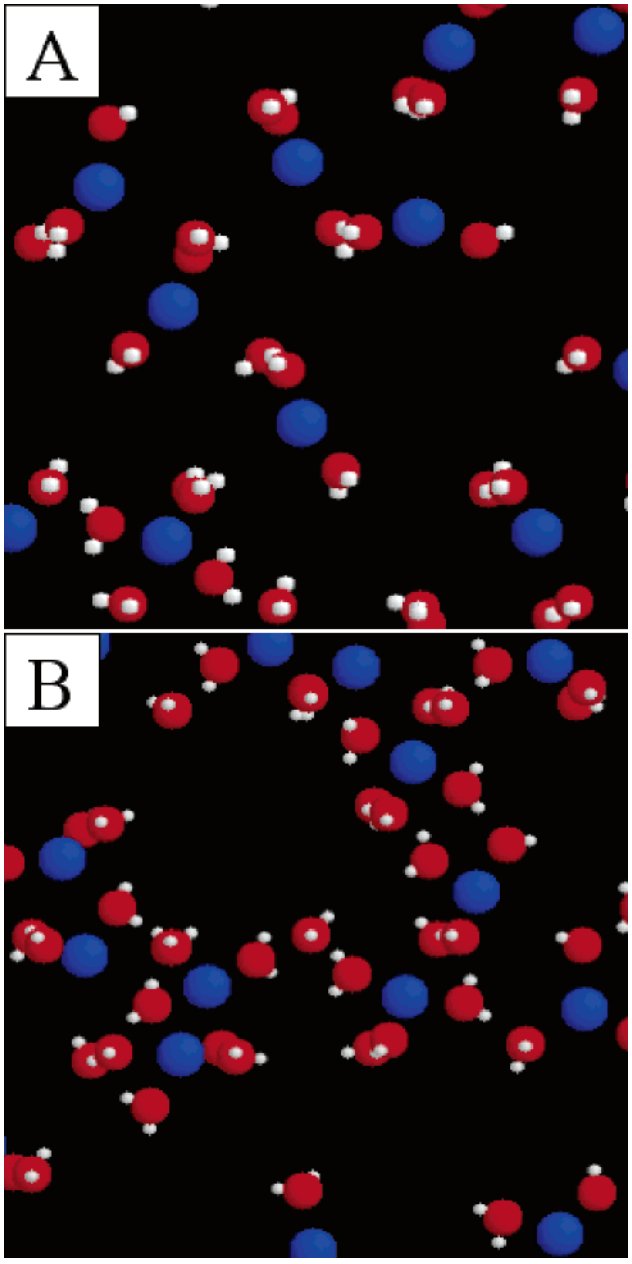

Figure 11. Organization of water molecules in the $a-b$ plane obtained from GC/MC simulations. (A) $P/P_0 = 0.10$. (B) $P/P_0 = 0.20$. Light gray: hydrogen, red: oxygen, blue: sodium.

GC/MC simulations performed for a relative pressure of 0.50 (Figure 13) are coherent with this latter picture and reveal important interactions between the clay layer and water molecules (Figures 13C,D). In addition, the existence of a percolat-

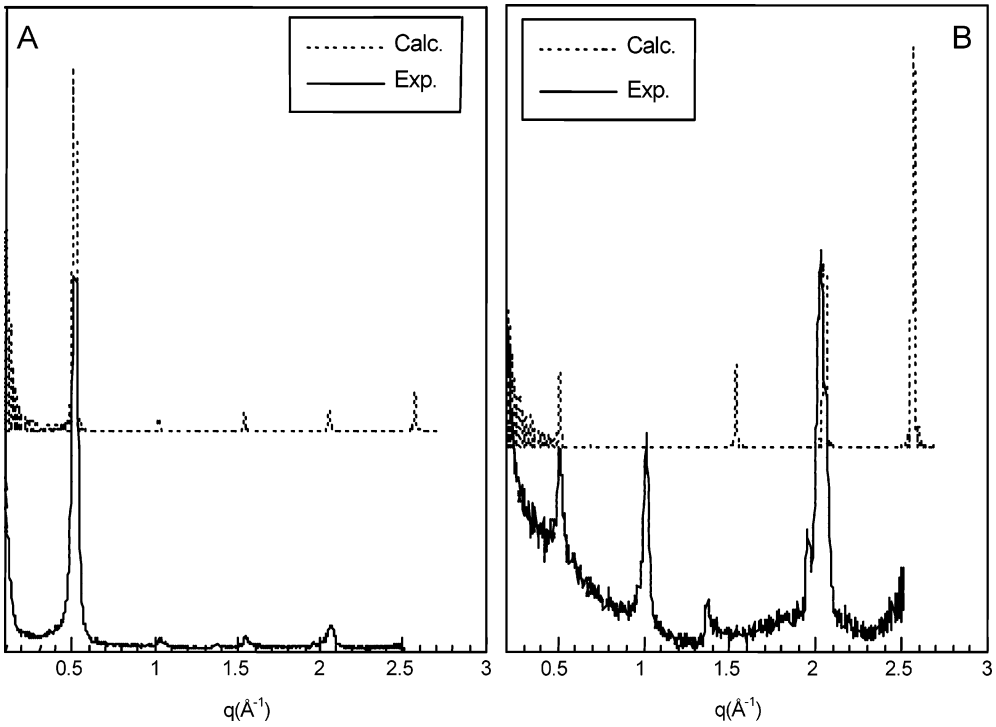

Figure 12. Comparison between experimental and calculated neutron diffraction patterns for a relative pressure of 0.20. (A) H_2O and (B) D_2O.

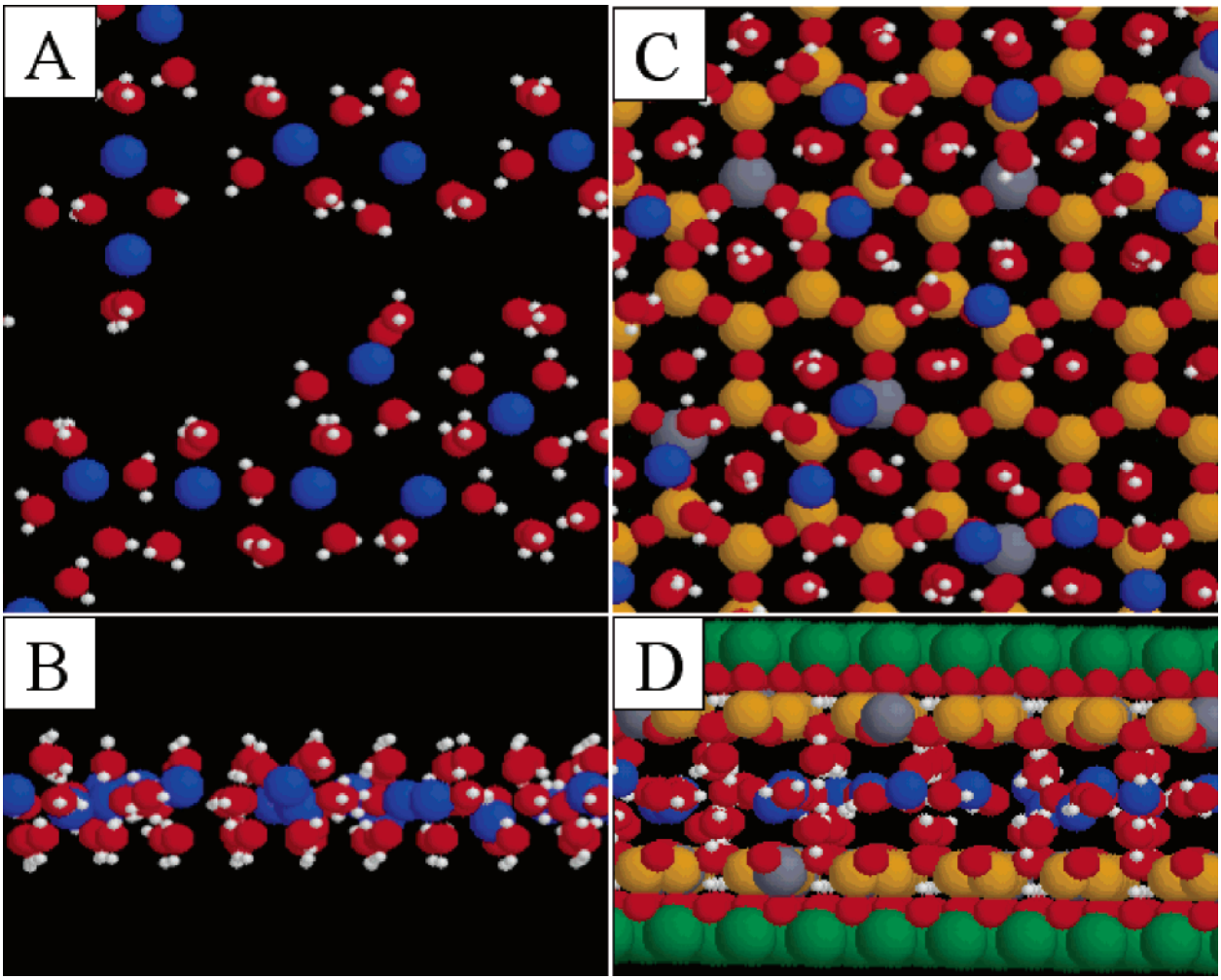

Figure 13. Organizations derived from GC/MC simulations for $P/P_0 = 0.50$. Light gray: hydrogen, red: oxygen, blue: sodium, beige: silicon, dark gray: aluminum, green: magnesium. (A) View of water in the $a-b$ plane. (B) View of water perpendicularly to the c axis. (C and D) Same as A and B with the clay layer.

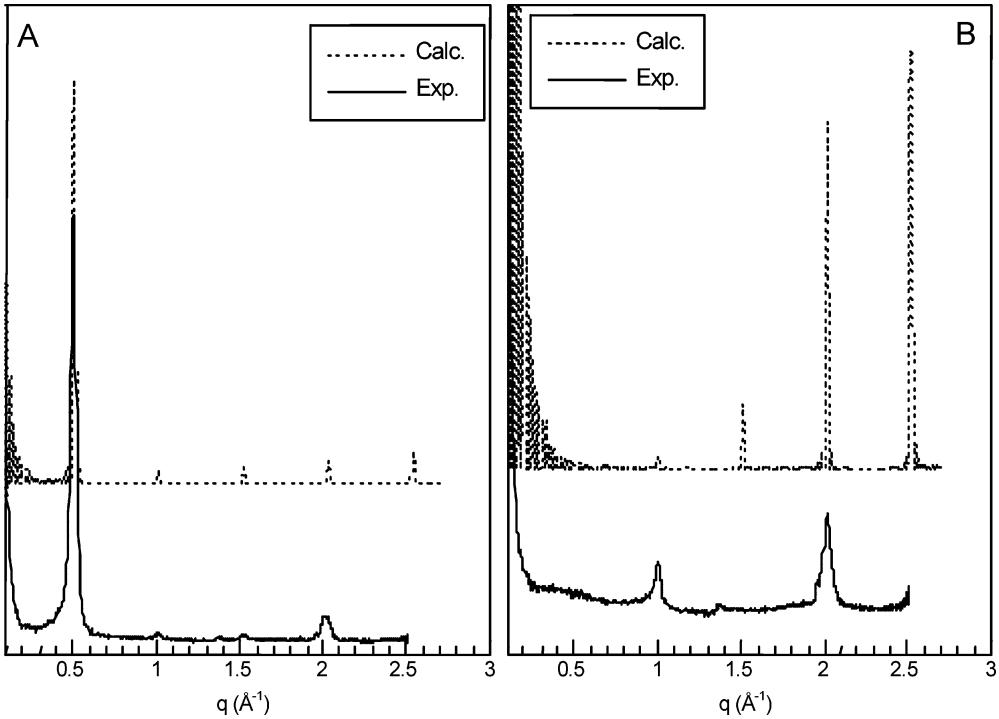

Figure 14. Comparison between experimental and calculated neutron diffraction patterns for relative pressures of 0.40 [(A) H_2O] and 0.50 [(B) D_2O].

ing hydrogen bond network can be observed in Figure 13A. This stage, where water appears strongly confined, corresponds to the complete extinction of the d_{001} line in the neutron D_2O diffraction patterns. Figure 14 presents a comparison between the experimental and calculated neutron diffraction patterns for H_2O at $P/P_0 = 0.40$ (Figure 14A) and for D_2O at $P/P_0 = 0.50$ (Figure 14B), i.e., at the closest points from the experimental conditions ($P/P_0^{\text{desorption}} = 0.25$ for H_2O and $P/P_0^{\text{desorption}} = 0.38$ for D_2O). As in the previous case for a relative pressure of 0.20, the calculated and experimental patterns match very well in the case of H_2O. In the case of D_2O, the complete extinction of the d_{001} line observed experimentally is perfectly reproduced in the calculated diagrams Still, as in the previous comparison (Figure 12), there is some minor discrepancy in the relative intensities of the various d_{001} lines between experimental and calculated patterns.

To better understand the molecular origin of the extinction of the d_{001} line in the neutron diffraction pattern (Figure 14B), let us assume an infinite stack of clay/water interfaces.[88] This approximation reduces eq 3b to

$$S_{00l} = \frac{1}{L}\int_{-L}^{L} G(z)\cos\left(\frac{\pi l z}{L}\right) \mathrm{d}z \qquad (4a)$$

with

$$G(z) = \sum_{j}^{N_{\text{wat}}+N_{\text{cat}}+N_{\text{at}}} f_j c_j(z) \qquad (4b)$$

where $2L$ is the period of the clay/water interface and $c_j(z)$ is the local density of atoms j. Note that the neutron atomic structure factors (f_j) are independent of the scattering length. This simplified procedure was shown to reproduce adequately the ratio of the line intensities of the neutron diffraction pattern, but obviously ignores the exact shape and width of the different lines. Figure 15A illustrates the atomic concentration profiles calculated by GC/MC simulation at $P/P_0 = 0.50$ for the water molecules and the sodium cations confined between the saponite sheets with a period of 12.47 Å. The profile thus obtained is close to that obtained by Skipper et al. in Llano Na-vermiculite (Figure 6 in ref 1a), on the basis of structural refinements of neutron diffraction spectra. The only difference lies in the depletion of H in the central position in vermiculite compared to that in saponite. This can be explained by the higher concentration in sodium cations in the mid-plane of vermiculite. The corresponding partial integrand $G(z)$ (eq 4a,b) is displayed in Figure 15B together with the contributions from the atoms of the clay network. By contrast with Figure 15A, the reference of the $G(z)$ function coincides with the layer of octahedral Mg sites. Finally, the complete integrand $G(z)$ *cos($\pi z/L$) (eq 4a,b) is also displayed in Figure 15B, illustrating how the interfacial content (amount, position, and orientation of the water molecules) may cancel the contribution from the atoms of the clay network. Note that the only atoms with a negative neutron scattering factor are the protons from the clay network that were shown not to exchange with those of the confined water molecules on the time scale of our experiments. As a consequence, the vanishing of the intensity of the d_{001} line is not related to any matching of the scattering lengths at both sides of the clay/water interface. The simultaneous reproduction of both H_2O and D_2O patterns is a strong constraint for GC/MC simulations. In particular, the extinction of the 001 line with D_2O *is extremely sensitive to both the positions and orientations of water molecules*. As a consequence, the picture derived from GC/MC simulations, though not perfect, is rather robust. It suggests hydrogen bonding between water molecules and clay surface oxygen atoms as well as significant interactions between water molecules and the center of the ditrigonal cavities. This provides a more precise picture of hydrated saponite than that previously obtained on the basis of X-ray diffraction and IR measurements.[14,72,73]

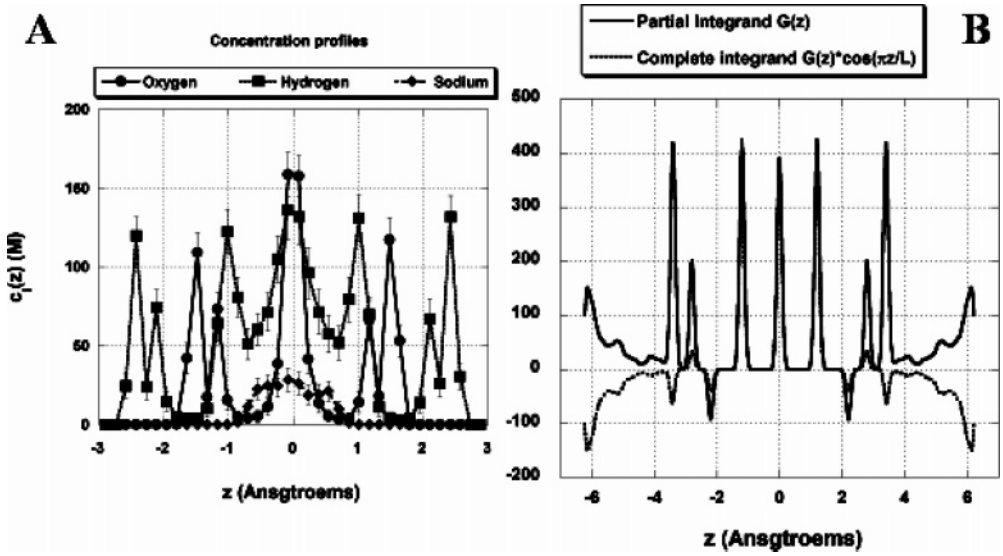

Figure 15. *d* spacing 12.47 Å at $P/P_0 = 0.50$. (A) Atomic concentration profiles of the confined water molecules and sodium counterions. (B) Integrand used to calculate the intensity of the neutron d_{001} diffraction line (see text).

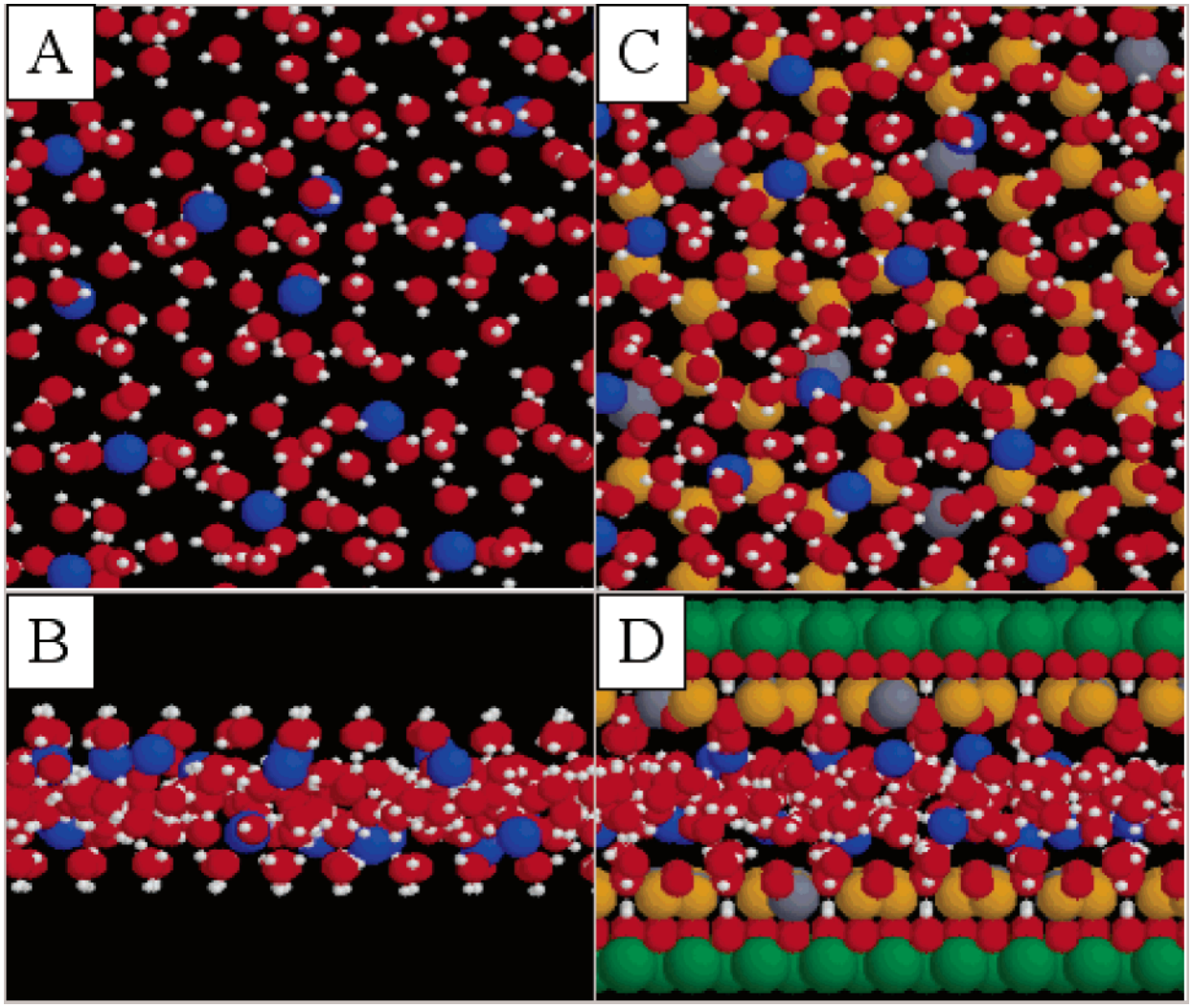

Figure 16. Organizations derived from GC/MC simulations for $P/P_0 = 0.80$. Light gray: hydrogen, red: oxygen, blue: sodium, beige: silicon, dark gray: aluminum, green: magnesium. (A) View of water in the $a-b$ plane. (B) View of water perpendicularly to the *c* axis. (C and D) Same as A and B with the clay layer.

Sixth Hydration Range. For relative pressures between 0.50 and ~0.80, the amount of water adsorbed increases sharply with the additional adsorption of the equivalent of around 4.5 molecules of water per sodium cation (Figure 1). In that range, the interlamellar distance also increases significantly to reach values of ~15.2 Å for a relative pressure of 0.80 (Figure 2). Such a discrete increase in basal spacing is typical of swelling clay minerals and has been observed in numerous studies. As

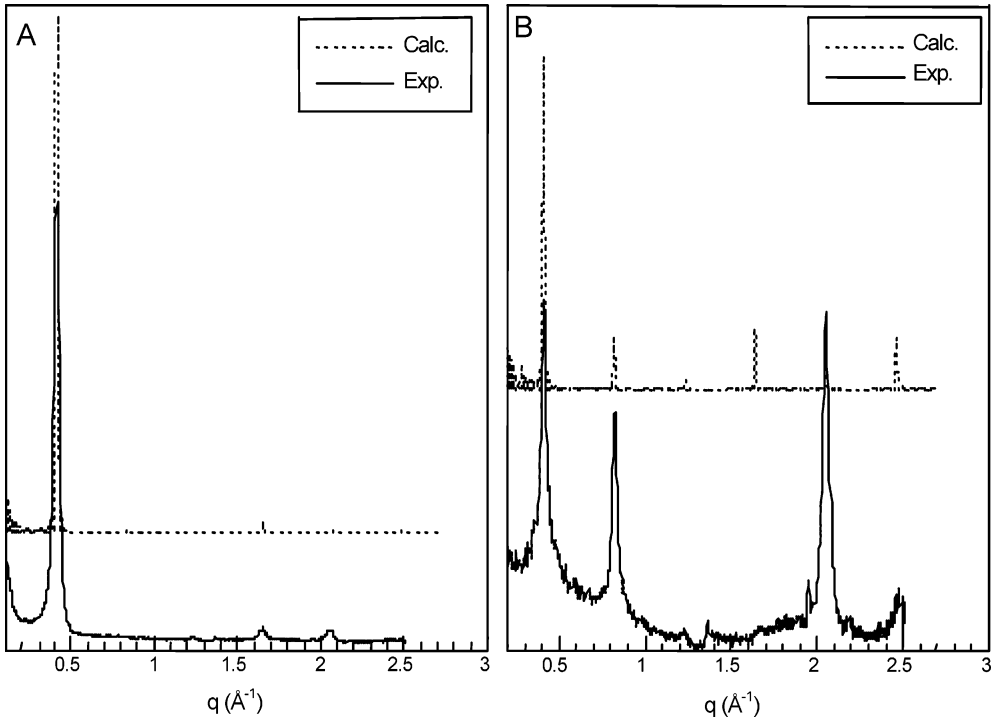

Figure 17. Comparison between experimental and calculated neutron diffraction patterns for a water relative pressure of 0.90. (A) H_2O and (B) D_2O.

already shown,[70−76] tetrahedral charge location sharpens the transition from the "one-layer hydrate" to the "two-layer hydrate". However, as already mentioned, detailed X-ray diffraction studies[87] have recently revealed the presence of interstratified states in the transition region. In that region, some minor discrepancies between the various techniques used to assess the amount of adsorbed water can be observed. Indeed, XRD experiments (Figure 2), NIR results (Figure 5), and GC/MC simulations (Figure 7) exhibit a sharper step than water adsorption gravimetric experiments (Figure 1). Static equilibrium tests carried out on various saponite samples have revealed[57] that, in this range of relative pressure, the quasi-equilibrium procedure used for gravimetric experiments tends to slightly underestimate the amount of water adsorbed and that the true shape of the step should be steeper than what is observed in Figure 1. In the spectral range corresponding to water signals, broad bands centered around 4900, 5160, 5240, and 5600 cm^{-1} grow (Figure 8B, difference ϕ). In parallel, in the range corresponding to water overtones and structural hydroxyls (Figure 9B, difference ϕ), broad signals centered around 6950 and 7400 cm^{-1} are observed together with a sharper band at 7190 cm^{-1}. All of the broad signals observed correspond to liquidlike water molecules. However, the full width of the massive is lower than that in bulk water,[80] which suggests that the network of interlayer water molecules is more structured than in bulk water. The band at 7190 cm^{-1} could be interpreted as corresponding to structural hydroxyl groups that are less perturbed than in the previous hydration stage, which could suggest that additional water molecules added in this hydration range are located less directly above ditrigonal cavities than in the previous hydration step.

The GC/MC simulations obtained for a relative pressure of 0.80 (Figure 16) are consistent with the data derived from NIR spectroscopic experiments. They also concur with the profile obtained on Na-vermiculite (Figure 4 in ref 1a). Indeed, liquidlike water molecules are observed (Figure 16A,B), whereas water molecules are less aligned with the ditrigonal cavities (Figure 16C,D) than in the previous hydration range (Figure 13C,D). In that range of water relative pressure, a significant hysteresis between adsorption and desorption branches was evidenced in the evolution of the interlamellar distances.[49] For that reason, a direct comparison between experimental neutron diffraction patterns obtained in desorption and calculated ones derived from GC/MC computations obtained in adsorption may not be fully relevant.

Seventh Hydration Range. For high relative pressure values above 0.80, the amount of water adsorbed (Figure 1) continues to increase strongly, whereas the X-ray diffraction patterns exhibit a constant d_{001} distance at 15.2 Å. In that range, the adsorption of water in the pores between clay particles starts to be significant, which can explain the discrepancy obtained between gravimetric and NIR measurements (Figures 1 and 5) that display a significant increase in the adsorbed amount and GC/MC simulations (Figure 7) that only lead to a moderate increase in adsorbed quantities. Compared with those in the previous hydration range, the NIR signals observed in the range between 4500 and 6000 cm^{-1} (Figure 8B, difference γ) are slightly modified as broad signals are observed around 5000 and 5190 cm^{-1} with shoulders at 5340 and 5650 cm^{-1}. In parallel, in the range between 6000 and 8000 cm^{-1} (Figure 9B, difference γ), broad bands centered around 6950 and 7400 cm^{-1} are observed together with a fine signal at 7190 cm^{-1} and a weak broader component centered around 7320 cm^{-1}. The shoulder at 5340 cm^{-1} and the signal at 7320 cm^{-1} characteristic of a water molecule with one of the two OH groups free of H-bonding correspond to a fundamental stretching vibration around 3730 cm^{-1}. Such a wavenumber is observed in the sum frequency generation (SFG) spectra obtained for aqueous solutions.[89−91] In our case, the two components at 5340 and 7320 cm^{-1} can then be assigned to water molecules located at the air/water interface in partially filled pores between clay particles. The results thus obtained confirm previous studies showing the importance of capillary condensation in interparticle

pores at high relative pressure[15,92,93] and provide a spectroscopic signature for water molecules in that environment.

The GC/MC simulation for a relative pressure of 0.90 is very close to that obtained for a relative pressure of 0.80 (Figure 16) and is therefore not presented. Still, it can be used for comparing experimental (Figure 3, $P/P_0^{\text{desorption}} = 0.84$) and calculated neutron H_2O and D_2O diffraction patterns (Figure 17). Once again, in the case of H_2O (Figure 17A), the agreement between experimental and calculated patterns is very good, whereas some discrepancy in relative intensities is observed for D_2O. As mentioned earlier, the difference between experimental and calculated spectra could certainly be used for refining the position and orientation of water molecules in the interlayer space of saponite clay.

V. Concluding Remarks

Using well-defined synthetic clay samples allows the study of in detail water adsorption by combining energetic, structural, and molecular information. In addition, such synthetic samples are well suited to perform molecular simulations that can be compared directly to experimental data. In the case of saponite with tetrahedral substitution, where cation/layer interactions are rather strong, swelling is initiated by cation/water interactions. However, the addition of at least three water molecules per cation is required to overcome the cation/layer interaction and displace the sodium cations toward the center of the interlayer region. A filling of the interlayer at nearly constant spacing then occurs to reach a well-organized network of interlayer water molecules with significant interactions with the clay layer. The structure thus formed leads to a complete extinction of the d_{001} line in D_2O neutron diffraction patterns. This shows, as initially suggested by Hawkins and Egelstaff,[10] that the classically used notion of a one-layer state for clay minerals is misleading for describing such a system. Upon further water adsorption, additional swelling is observed for $P/P_0 > 0.5$, and a network of liquidlike water molecules more structured than in bulk water is then present in the interlayer region.

In view of the interplay between cation/water, cation/layer, and water/layer interactions, it would be very relevant to modify these various interactions by changing layer charge, temperature, and the nature of the exchangeable cation. Such studies are currently underway and will be the object of further publications. A description of clay/water systems should also be completed by working on synthetic samples with octahedral substitution in which cation/layer interactions should be very different from that of tetrahedrally charged samples such as saponite. Furthermore, as the present study provides detailed snapshots of water and cation organization increasing water chemical potential, combined numerical and experimental investigations should be implemented to determine the dynamics of the system at various timescales.

Acknowledgment. This research is a part of a Ph.D. study initiated, followed, and supported by Andra (Agence nationale pour la gestion des déchets radioactifs), the French national radioactive waste management agency, in the framework of its program on the geochemical behavior of bentonite engineered barrier. A.D. cordially thank Drs. P. Andreazza, N. Cohaut, and I. Rannou for helpful discussions. GC/MC simulations were performed either locally on workstations purchased thanks to grants from Région Centre (France) or on the Nec supercomputer (IDRIS, Orsay, France).

References and Notes

(1) A lot of work [e.g., (a). Skipper, N. T.; Soper, A. K.; McConnell, J. D. C. *J. Chem. Phys.* **1991**, *94*, 5751. (b) Skipper, N. T.; Sposito, G.; Fang R. C. C. *Clays Clay Miner.* **1997**, *43*, 294 (c) Arab, M.; Bougeard, D.; Smirnov, K. S. *Phys. Chem. Chem. Phys.* **2004**, *6*, 2446] has also been dedicated to vermiculite that presents mainly tetrahedral substitution. However, the layer charge of vermiculite is much higher than that of smectites sensu stricto.

(2) Cases, J. M.; Berend, I.; Besson, G.; François, M.; Uriot, J. P.; Thomas, F.; Poirier, J. E. *Langmuir* **1992**, *8*, 2730.

(3) Berend, I.; Cases, J. M.; François, M.; Uriot, J. P.; Michot, L. J.; Masion, A.; Thomas, F. *Clays Clay Miner.* **1995**, *43*, 324.

(4) Cases, J. M.; Berend, I.; François, M.; Uriot, J. P.; Michot, L. J.; Thomas, F. *Clays Clay Miner.* **1997**, *45*, 8.

(5) Mooney, R. W.; Keenan, A. G.; Wood, L. A. *J. Am. Chem. Soc.* **1952**, *74*, 1371.

(6) Norrish, K. *Discuss. Faraday Soc.* **1954**, *18*, 120.

(7) Omerod, E. C.; Newman, A. C. D. *Clay Miner.* **1983**, *18*, 289.

(8) Cebula, D. J.; Thomas, R. K.; Middleton, S.; Ottewill, R. H.; White, J. W. *Clays Clay Miner.* **1979**, *27*, 39.

(9) Powell, D. H.; Tongkhao, K.; Kennedy, S. J.; Slade, P. G. *Clays Clay Miner.* **1997**, *45*, 290.

(10) Hawkins, R. K.; Egelstaff, P. A. *Clays Clay Miner.* **1980**, *28*, 19.

(11) Farmer, V. C.; Russell, J. D. *Trans. Faraday Soc.* **1971**, *67*, 2737.

(12) Prost, R. *Ann. Agron.* **1975**, *26*, 463.

(13) Cariati, F.; Erre, L.; Micera, G.; Piu, P.; Gessa, C. *Clays Clay Miner.* **1981**, *29*, 157.

(14) Sposito, G.; Prost, R. *Chem. Rev.* **1982**, *82*, 553.

(15) Johnston, C. T.; Sposito, G.; Erickson, C. *Clays Clay Miner.* **1992**, *40*, 722.

(16) Bishop, J. L.; Pieters, C. M.; Edwards, J. O. *Clays Clay Miner.* **1994**, *42*, 702.

(17) Pelletier, M.; Thomas, F.; de Donato, P.; Michot, L. J.; Cases, J. M. *Clays For Our Future.* Proceedings of the 11th International Clay Conference; Kodama, H., Mermut, A. R., Torrance, J. C., Eds.; Ottawa (Canada), 1999; p 555.

(18) Conard, J. *Magnetic Resonance in Colloid and Interface Science*; ACS Symposium Series 34; American Chemical Society: Washington, DC, 1976; p 85.

(19) Woessner, D. E. *J. Magn. Reson.* **1980**, *39*, 297.

(20) Grandjean, J.; Laszlo, P. *Clays Clay Miner.* **1989**, *37*, 403.

(21) Delville, A.; Grandjean, J.; Laszlo, P. *J. Phys. Chem.* **1991**, *95*, 1383.

(22) Weiss, C. A., Jr.; Gerasimowicz, W. V. *Geochim. Cosmochim. Acta* **1996**, *60*, 265.

(23) Poinsignon, C.; Estrade-Schwarzckopf, J.; Conard, J.; Dianoux, A. J. *Proc. Intl. Clay Conf.*; Schultz, L. G., Van Olphen, H., Mumpton, F. A., Eds.; The Clay Minerals Society, 1987; p 284.

(24) Poinsignon, C. *Solid State Ionics* **1997**, *97*, 399.

(25) Mamy, J. Ph.D. Thesis, INRA, Paris, France, 1968.

(26) Belarbi, H.; Haouzi, A.; Giuntini, J. C.; Zanchetta, J. V.; Niezette, J.; Vanderschueren, J. *Clay Miner.* **1997**, *32*, 13.

(27) Haouzi, A.; Kharroubi, M.; Belarbi, H.; Devautour-Vinot, S.; Henn, F.; Giuntini, J. C. *Appl. Clay Sci.* **2004**, *27*, 67.

(28) Fripiat, J. J.; Cases, J. M.; François, M.; Letellier, M. *J. Colloid Interface Sci.* **1982**, *89*, 378.

(29) Delville, A.; Letellier, M. *Langmuir* **1995**, *11*, 1361.

(30) Nakashima, Y. *Clays Clay Miner.* **2003**, *51*, 9.

(31) Porion, P.; Al Mukhtar, M.; Faugère, A. M.; Pellenq, R. J. M.; Meyer, S.; Delville, A. *J. Phys. Chem. B* **2003**, *107*, 4012.

(32) Delville, A. *Langmuir* **1992**, *8*, 1796.

(33) Boek, E. S.; Coveney, P. V.; Skipper, N. T. *Langmuir* **1995**, *11*, 4629.

(34) Boek, E. S.; Coveney, P. V.; Skipper, N. T. *J. Am. Chem. Soc.* **1995**, *117*, 12608.

(35) Chang, F. R. C.; Skipper, N. T.; Sposito, G. *Langmuir* **1995**, *11*, 2734.

(36) Delville, A. *J. Phys. Chem. B* **1995**, *99*, 2033.

(37) Sposito, G.; Park, S. H.; Sutton, R. *Clays Clay Miner.* **1999**, *47*, 192.

(38) Young, D. A.; Smith, D. E. *J. Phys. Chem. B* **2000**, *104*, 9163.

(39) Hensen, E. J. M.; Tambach, T. J.; Bliek, A.; Smit, B. *J. Chem. Phys.* **2001**, *115*, 3322.

(40) Marry, V.; Turq, P. *J. Phys. Chem. B* **2003**, *107*, 1832.

(41) Boek, E. S.; Sprik, M. *J. Phys. Chem. B* **2003**, *107*, 3251.

(42) Eypert-Blaison, C.; Michot, L. J.; Humbert, B.; Pelletier, M.; Villiéras, F.; d'Espinose de la Caillerie, J.-B. *J. Phys. Chem. B* **2002**, *106*, 730.

(43) Michot, L. J.; Villiéras, F.; Lambert, J.-F.; Bergaoui, L.; Grillet, Y.; Robert, J.-L. *J. Phys. Chem. B* **1998**, *102*, 3466.

(44) Lartiges, B. S.; Chaignon, V.; Michot, L. J.; Robert, J.-L. *Water Sci. Technol.* **1998**, *38*, 319.

(45) Thomas, F.; Michot, L. J.; Vantelon, D.; Montargès, E.; Prélot, B.; Cruchaudet, M.; Delon, J.-F. *Colloids Surf., A* **1999**, *159*, 351.

(46) Pelletier, M.; Michot, L. J.; Barrès, O.; Humbert, B.; Petit, S.; Robert, J.-L. *Clay Miner.* **1999**, *34*, 439.

(47) Michot, L. J.; Villiéras, F. *Clay Miner.* **2002**, *37*, 39.
(48) Pelletier, M.; Michot, L. J.; Humbert, B.; Barrès, O.; d'Espinose de la Caillerie, J.-B.; Robert, J.-L. *Am. Mineral.* **2003**, *88*, 1801.
(49) Michot, L. J.; Bihannic, I.; Pelletier, M.; Rinnert, E.; Robert, J.-L. *Am. Mineral.* **2005**, *90*, 166.
(50) Hamilton, D. L.; Henderson, C. M. B. *Mineral. Magn.* **1968**, *36*, 832.
(51) Delevoye, L.; Robert, J.-L.; Grandjean, J. *Clay Miner.* **2003**, *38*, 63.
(52) Poirier, J. E.; François, M.; Cases, J. M.; Rouquerol, J. *Proceedings of the Second Engineering Foundation Conference on Fundamentals of Adsorption*; Liapis, A. I., Ed.; AIChE. Pub: New York, 1987; p 473.
(53) Perino-Gallice, L.; Fragneto, G.; Mennicke, U.; Salditt, T.; Rieutord, F. *Eur. Phys. J. E* **2002**, *8*, 275.
(54) Durocher, G.; Sandorfy, C. *J. Mol. Spectrosc.* **1965**, *15*, 22.
(55) Carteret, C. Ph.D. Thesis, University Henri Poincaré, Nancy, France, 1999.
(56) Carteret, C.; Burneau, A. Near Infrared Characterization of Silicas. In *Silica 98: An International Conference on Silica Science and Technology*; Mulhouse: France, 1998; p 743.
(57) Rinnert, E. Ph.D. Thesis, University Henri Poincaré, Nancy, France, 2004.
(58) Rinnert, E.; Carteret, C.; Humbert, B.; Michot, L. J. *Appl. Spectrosc.* **2005**. Manuscript submitted.
(59) Adams, D. J. *Mol. Phys.* **1974**, *5*, 1241.
(60) Allen, M. P.; Tildesley, D. J. *Computer Simulation of Liquids*; Clarendon Press: Oxford, 1994.
(61) Pabst, A. *Am. Mineral.* **1955**, *40*, 967.
(62) Van Gunsteren, W. F.; Berendsen, H. J. C.; Rullmann, J. A. C. *Mol. Phys.* **1981**, *44*, 69.
(63) Jorgensen, W. L.; Chandrasekhar, J.; Madura, J.; Impey, R. W.; Klein, M. L. *J. Chem. Phys.* **1983**, *79*, 926.
(64) Bounds, D. G. *Mol. Phys.* **1985**, *54*, 1335.
(65) Heyes, D. M. *Phys. Rev. B* **1994**, *49*, 755.
(66) Hummer, G. *Chem. Phys. Lett.* **1995**, *235*, 297.
(67) Macgillavry, C. H.; Rieck, G. D.; Lonsdale, K. *Physical and Chemical Tables*; International Tables for X-ray Crystallography, Vol III; The Knynoch Press: Birmingham, 1962.
(68) Drits, V. A.; Tchoubar, C. X-ray Diffraction by Disordered Lamellar Structure. In *Theory and Applications to Microdivided Silicates and Carbons*; Springer-Verlag: Berlin, 1990.
(69) Zevin, L. S.; Kimmel, G. *Quantitative X-ray Diffractometry*; Springer: New York, 1995.
(70) Glaeser, R.; Méring, J. *C. R. Acad. Sci., Ser. D* **1968**, *267*, 463.
(71) Suquet, H.; de la Calle, C.; Pézerat, H. *Clays Clay Miner.* **1975**, *23*, 1.
(72) Suquet, H.; Iiyama, J. T.; Kodama, H.; Pézerat, H. *Clays Clay Miner.* **1977**, *25*, 231.
(73) Suquet, H.; Prost, R.; Pézerat, R. *Clay Miner.* **1982**, *17*, 225.
(74) Ben Brahim, J.; Besson, G.; Tchoubar, C. *J. Appl. Crystallogr.* **1984**, *17*, 179.
(75) Ben Brahim, J.; Armagan, N.; Besson, G.; Tchoubar, C. *Clay Miner.* **1986**, *21*, 111.
(76) Suquet, H.; Pézerat, H. *Clays Clay Miner.* **1987**, *35*, 353.
(77) Zettlemoyer, A. C.; Hsing, H. H. *J. Colloid Interface Sci.* **1976**, *55*, 637.
(78) Burneau, A.; Gallas, J. P. *The Surface Properties of Silicas*; Legrand, A. P., Ed.; John Wiley & Sons: New York, 1998; p 147.
(79) Burneau, A.; Barrès, O.; Gallas, J. P.; Lavalley, J. C. *Langmuir* **1990**, *6*, 1364.
(80) Burneau, A. Ph.D. Thesis, University Paris VI., 1973.
(81) Benedict, W. S.; Gailar, N.; Plyler, E. K. *J. Chem. Phys.* **1956**, *24*, 1139.
(82) Hagymassy, J. S.; Brunauer, S.; Mikhail, R. S. *J. Colloid Interface Sci.* **1969**, *29*, 485.
(83) Laird, D. A. *Clays Clay Miner.* **1999**, *47*, 630.
(84) Russell, J. D.; Farmer, V. C.; Velde, B. *Mineral. Magn.* **1970**, *37*, 869.
(85) Rosasco, G. J.; Blaha, J. J. *Appl. Spectrosc.* **1980**, *34*, 140.
(86) Sposito, G.; Prost, R.; Gaultier, J.-P. *Clays Clay Miner.* **1983**, *31*, 9.
(87) Ferrage E. Ph.D. Thesis, University Joseph Fourier, Grenoble, France, 2004.
(88) Skipper, N. T.; Smalley, M. V.; Williams, G. D.; Soper, A.; Thompson, C. H. *J. Phys. Chem.* **1995**, *99*, 14201.
(89) Baldelli, S.; Schnitzer, C.; Campbell, D. J.; Shultz M. J. *J. Phys. Chem. B* **1999**, *103*, 2789.
(90) Schnitzer, C.; Baldelli, S.; Campbell, D. J.; Shultz, M. J. *J. Phys. Chem. A* **1999**, *103*, 6383.
(91) Schnitzer, C.; Baldelli, S.; Shultz, M. J. *J. Phys. Chem. B* **2000**, *104*, 585.
(92) Prost, R.; Koutit, T.; Benchara, A.; Huard, E. *Clays Clay Miner.* **1998**, *46*, 117.
(93) Al-Mukhtar, M.; Qi, Y.; Alcover, J.-F.; Conard, J.; Bergaya, F. *Clay Miner.* **2000**, *35*, 537.